AGU PUBLICATIONS

JGR

Journal of Geophysical Research: Oceans

RESEARCH ARTICLE

10.1002/2016JC011757

Wind-driven export of Weddell Sea slope water

A. J. S. Meijers[1], M. P. Meredith[2], E. P. Abrahamsen[1], M. A. Morales Maqueda[3,4], D. C. Jones[1], and A. C. Naveira Garabato[5]

[1]British Antarctic Survey, High Cross, Cambridge, UK, [2]Scottish Association for Marine Science, Oban, UK, [3]School of Marine Science and Technology, Newcastle, UK, [4]National Oceanography Centre, Liverpool, UK, [5]University of Southampton, Southampton, UK

Key Points:
- High temporal resolution bottom observations of Antarctic Slope Current extension are made
- Export properties from the Weddell Sea are well correlated with changes of wind stress curl over the Weddell Gyre
- Export time scales indicate a 1–5 month lag between changes in winds and boundary current response in the Weddell Gyre

Correspondence to:
A. J. S. Meijers,
andmei@bas.ac.uk

Citation:
Meijers, A. J. S., M. P. Meredith, E. P. Abrahamsen, M. A. Morales Maqueda, D. C. Jones, and A. C. Naveira Garabato (2016), Wind-driven export of Weddell Sea slope water, *J. Geophys. Res. Oceans*, *121*, 7530–7546, doi:10.1002/2016JC011757.

Received 26 FEB 2016
Accepted 15 SEP 2016
Accepted article online 21 SEP 2016
Published online 17 OCT 2016

Abstract The export of waters from the Weddell Gyre to lower latitudes is an integral component of the southern subpolar contribution to the three-dimensional oceanic circulation. Here we use more than 20 years of repeat hydrographic data on the continental slope on the northern tip of the Antarctic Peninsula and 5 years of bottom lander data on the slope at 1000 m to show the intermittent presence of a relatively cold, fresh, westward flowing current. This is often bottom-intensified between 600 and 2000 dbar with velocities of over 20 cm s^{-1}, transporting an average of 1.5 ± 1.5 Sv. By comparison with hydrography on the continental slope within the Weddell Sea and modeled tracer release experiments we show that this slope current is an extension of the Antarctic Slope Current that has crossed the South Scotia Ridge west of Orkney Plateau. On monthly to interannual time scales the density of the slope current is negatively correlated ($r > 0.6$ with a significance of over 95%) with eastward wind stress over the northern Weddell Sea, but lagging it by 6–13 months. This relationship holds in both the high temporal resolution bottom lander time series and the 20+ year annual hydrographic occupations and agrees with Weddell Sea export variability observed further east. We compare several alternative hypotheses for this wind stress/export relationship and find that it is most consistent with wind-driven acceleration of the gyre boundary current, possibly modulated by eddy dynamics, and represents a mechanism by which climatic perturbations can be rapidly transmitted as fluctuations in the supply of intermediate-level waters to lower latitudes.

1. Introduction

The Weddell Sea is a key formation region for the dense water masses that make up the lower cell of the global overturning circulation [*Marshall and Speer*, 2012]. These water masses are exported from the northern flank of the cyclonic Weddell Gyre into the Antarctic Circumpolar Current (ACC), and from there spread to much of the rest of the global ocean. Dense water subduction around the Antarctic continent forms a relatively rapid pathway between atmosphere and ocean interior for the sequestration of heat and CO_2 on long (centennial to millennial) time scales, and consequently is an important factor in the global climate and sea level. The impact of changes in these deep waters on sea level has been observed on decadal time scales [*Purkey and Johnson*, 2013] and variability in deep water mass carbon and volume invoked as drivers in glacial/interglacial transitions [*Watson and Naveira Garabato*, 2006]. Because dense waters tend to be formed in relatively small geographic locations over the continental shelf, they are likely to be susceptible to changes in forcing associated with both natural and anthropogenic climate change. Understanding this potential variability is a significant challenge for climate modeling [*Meijers*, 2014].

Dense water export from the Weddell Gyre to the Scotia Sea and ACC has received significant attention in recent years [e.g., *Meredith et al.*, 2004; *Garabato et al.*, 2002; *Meredith et al.*, 2011; *Palmer et al.*, 2012]. The exact pathway of dense waters from the gyre to the ACC is heavily influenced by the presence of intervening topography, most notably the South Scotia Ridge running eastward from the tip of the Antarctic Peninsula (Figure 1). This ridge generally reaches to within 1500 m of the surface and blocks the denser water masses; Lower Weddell Sea Deep water (LWSDW $\gamma_n > 28.31$ kg m^{-3}) and Upper Weddell Sea Deep water (UWSDW, $28.26 < \gamma_n < 28.31$ kg m^{-3}) from entering the Scotia Sea [*Garabato et al.*, 2002]. However, in a few locations deep passages in the South Scotia Ridge permit the export of these dense waters from the Weddell to the Scotia Sea. The deepest of these is Orkney Passage (3500 m) east of the Orkney Plateau [*Gordon et al.*, 2001], but several others such as Philip Passage (1900 m) exist closer to the peninsula west of

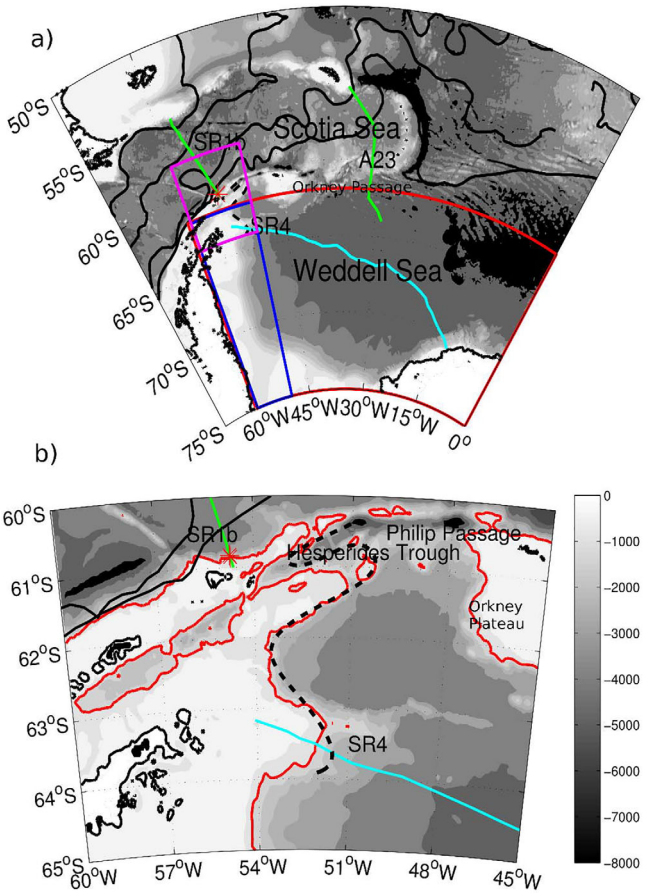

Figure 1. Features of the (a) wider study area and (b) region of interest around the bottom landers (red stars). Mean position of the major hydrographic features are indicated in bold lines (from north to south: SubAntarctic Front, Polar Front, Southern Antarctic Circumpolar Front, Southern Boundary) while the color map is bathymetry. The pathway of Antarctic Slope Front is given by the dashed line, based on *Heywood et al*. [2004]. The SR1b and A23 transects are shown in green and the SR4 in cyan, and the 1000 m isobath is indicated in red. Colored boxes in Figure 1a indicate integration regions for wind stress curl (see section 3.2).

Orkney Plateau. While the majority of the exported WSDW spreads eastward, following the main flow direction of the ACC [*Patterson and Sievers*, 1980], *Garabato et al*. [2002] note the presence of WSDW within Drake Passage as far west as 64°W. Within this WSDW they observe two distinct temperature/salinity classes and suggest that the difference supports the hypothesis of *Nowlin and Zenk* [1988] that in addition to Orkney Passage another pathway exists west of Orkney Plateau, with subsequent westward transport north of the peninsula. These exit pathways were quantified by *Heywood et al*. [2004] who show that the Antarctic Slope Current (ASC) that forms the western boundary current of the Weddell Gyre divides upon encountering the South Scotia Ridge, with one limb of around 7 Sv crossing the ridge west of Orkney Plateau and the remainder (13 Sv) carrying on south of Orkney Plateau as the Weddell Front (the northern boundary of the Weddell gyre) and ultimately exiting via Orkney Passage. That study notes that the ultimate fate of the ASC after crossing the ridge is unknown, but suggests that it may flow eastward.

The properties of the exported WSDW within the Scotia Sea have been observed to change over the last two decades of observations in volume and temperature/salinity characteristics, both within the western (Drake Passage/SR1b WOCE section) and eastern (A23 section) portions of the Scotia basin. The denser LWSDW has a clear freshening trend and has significantly reduced in volume since 1993 [*Jullion et al*., 2013]. The lighter class, UWSDW, has exhibited more variability over the Scotia Sea. It was observed to warm and increase in salinity between 1994 and 1999 [*Meredith et al*., 2008] followed by a cooling and freshening to 2007 and then a recovery to near original levels by 2012 [*Jullion et al*., 2013]. *Meredith et al*. [2008] hypothesized that this variability may be driven by a change in the baroclinicity of the Weddell Gyre in response to changes in the cyclonic wind stress curl that sets the gyre intensity [*Martinson and Iannuzzi*, 2003]. A baroclinic spin-up (down) of the gyre would act to deepen (shoal) the intersections of isopycnals with the Scotia ridge sills, thus increasing (decreasing) the flow of relatively warmer waters from the gyre to Scotia Sea.

Subsequently, observations were made that informed on the time lag between changes in atmospheric forcing over the Weddell Gyre and the response of WSDW properties within the Scotia Sea and Drake Passage [*Jullion et al*., 2010; *Meredith et al*., 2011]. These lags were surprisingly short (order of just a few months), and while the baroclinic response time of a subpolar gyre is not well constrained, classical theory postulates a time scale of several years [e.g., *Anderson and Gill*, 1975]. Consequently, other hypotheses were examined to explain the rapid response observed. *Meredith et al*. [2011] and *Polzin et al*. [2014] suggest that the change in isopycnal depth at the South Scotia Ridge may instead be driven by bottom Ekman layer

responses to barotropic spin-up/down of the gyre, in turn driven by wind stress curl forcing. In this mechanism an acceleration of the barotropic slope current would increase downslope Ekman transport and therefore deepen isopycnal surfaces at the gyre boundary. *Thompson et al*. [2014] infers from observations in the north-west Weddell Sea that the necessary transport to support such increased Ekman flow at the gyre boundary may be supplied by middepth eddy transport across the gyre boundary current. This eddy mechanism is supported by idealized modeling and *Su et al*. [2014] suggest that mesoscale eddy mixing may drive significant isopycnal depth variability at the Weddell gyre boundaries in response to changes in surface Ekman pumping, and may do so on time scales of a few months.

Here we examine an export pathway from the Weddell Sea to the Scotia Sea using both long-term hydrographic observations extending back to 1993, as well as a unique 5 year high temporal resolution time series set within an extension of the Antarctic Slope Current (ASC) at the northern tip of the Antarctic Peninsula. We link the observed property variability at the bottom lander within the outflow region to changes in wind stress forcing over the wider Weddell Gyre and show that this relationship can be extended over the full hydrographic section time series, despite its relatively poor temporal resolution. We then examine the outflow variability in terms of wider Scotia Sea WSDW property change and discuss the candidate mechanisms that can link gyre spin-up/down to export property variability.

2. Data and Methods

2.1. Observations

2.1.1. Hydrography

The SR1b hydrographic section extends across Drake Passage and has been occupied to full depth 22 times since November 1993, with all occupations occurring in austral summer between November and March (see *Jullion et al*. [2013, Table 1] for details on transect timing and instrumentation). The section extends from Burdwood Bank, due south of the Falkland Islands, to Elephant Island near the northern tip of the Antarctic Peninsula (Figure 1). In this study we focus on the southern SR1b stations over the continental slope. These are positioned with spacing varying between 2 and 40 km so as to resolve the bathymetry. From 1993 to 1998 CTD observations were made using a Neil Brown Instruments MkIIIc CTD, with data checked and calibrated using temperature data from reversing thermometers and salinity data from discrete samples analyzed on an Autosal 8400B salinometer, while from 1999 onward a SBE35 CTD resolving the water column at 1–2 dbar was employed. Detailed data processing notes for voyages may be found in individual cruise reports (https://www.bodc.ac.uk/data/information_and_inventories/cruise_inventory/), and several studies have investigated the error of the data set as a whole [*Williams et al*., 2006; *Naveira Garabato et al*., 2009; *Jullion et al*., 2013]. They show that potential temperature (θ) have a systematic and standard error of 0.001°C, while for practical salinity (S_P) these errors are 0.002 and 0.001, respectively. Sampling error imposed by limited horizontal or vertical resolution have been estimated by subsampling well-resolved sections and regridding, and show errors of 0.002 S_P and 0.002°C at depth, although this value increases toward the surface [*Jullion et al*., 2013]. Repeat hydrography from the western end of the SR4 hydrographic section over the Weddell Sea continental shelf (Figure 1) was also used. This data have accuracies of 0.003°C and 0.003 S_P for temperature and salinity, respectively, although the consistency of water masses in this sector suggest accuracies may be as good as 0.001°C and 0.001 S_P [*Fahrbach et al*., 2004].

Processed data from Lowered Acoustic Doppler Current Profilers (LADCP) mounted on the CTD frame is available on 13 of the SR1b sections. The LADCP system comprises either one or two (varying between voyages) 300 kHz Teledyne RDI ADCPs mounted on the CTD frame. Horizontal velocities and their corresponding vertical shears were obtained from the CTD/LADCP data using the LDEO implementation of the velocity-inversion method [*Visbeck*, 2002] (available at http://www.ldeo.columbia.edu/~ant/LADCP). To obtain absolute velocity profiles, the downcast and upcast data were combined and velocity referencing was accomplished using bottom-track data, shipboard-ADCP, and vessel global positioning system (GPS) information. Processing varies slightly between voyages and over time and details may be found in individual cruise reports, but overall horizontal velocity errors over the slope are typically in the range 0.02–0.05 m s^{-1}.

2.1.2. Bottom Lander Data

Since 1992, a lander incorporating bottom pressure recorders (BPR) has been maintained on the Antarctic continental slope at the southern end of SR1b at 60°51.01′S, 54°42.64′W (Figure 1) around 1000 dbar

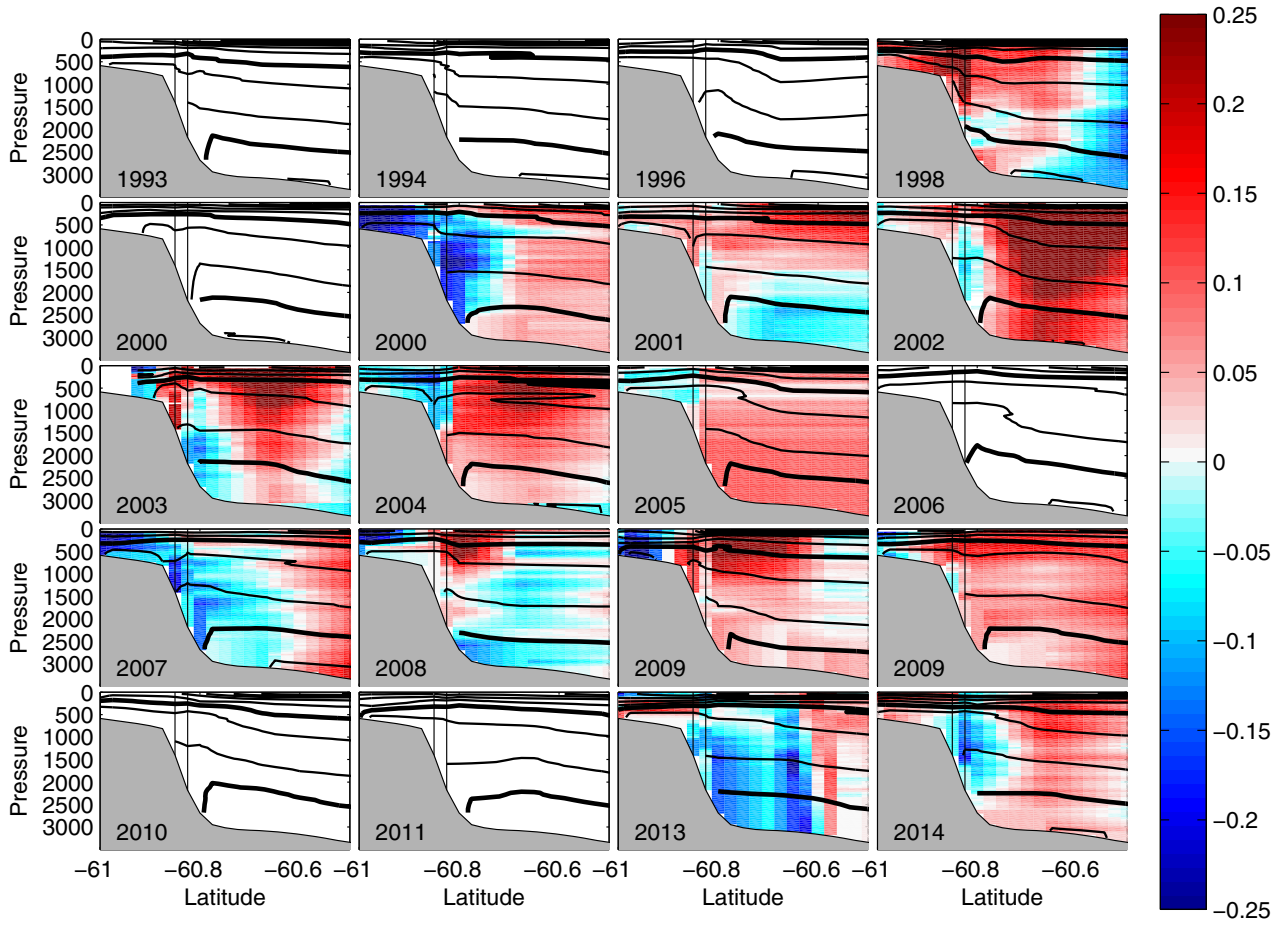

Figure 2. Neutral density (contours) and zonal velocity (color map) at the Antarctic continental slope section of SR1b for each occupation since 1993. Neutral density is given in 0.01 kg m^{-3} increments, with the bold lines indicating γ_n 28.2 and 28.26 kg m^{-3}. Positive velocity values are eastward. Black vertical lines indicate the latitude of the two bottom landers discussed in section 2.1.2. Sections with no color have no LADCP data available, but their neutral density is included for completeness.

[*Spencer et al.*, 1993; *Meredith et al.*, 2004]. From December 2006 to December 2011, the BPR landers were instrumented with one Sea-Bird Electronics microCAT SBE 37 measuring conductivity and temperature at 15 min interval with nominal accuracies of 0.0003 Sm^{-1} and 0.002°C, respectively. This instrument was recovered and redeployed in December 2009. A second BPR and SBE 37 lander was also deployed 3 km further north of the former, targeting the 2000 m isobath, from November 2009 to December 2011. The position of the two landers with respect to slope topography is shown in Figure 2. All microCATs were deployed fresh from recalibration by the manufacturer. No statistically significant drift in pressure occurs in either of the shallow bottom lander deployments, and despite a 100 dbar difference in bottom lander pressure (due to the very steep bathymetry in the region, despite identical release locations) the offset discontinuity in temperature and conductivity is negligible relative to local temporal variability. Differences in mean temperature and salinity exist between the two shallow time series, but these are likely due to an overall warming and salinification trend at the site over the deployment period and is supported by SR1b CTD observations (see section 3.1). A pressure trend of approximately 0.25 dbar/yr is present in the deep bottom lander, and is not constant throughout the deployment. It has not been corrected for, but even if it is spurious sensor drift this pressure trend would induce a change over the whole deployment of only 0.001°C and 0.0005 S_P, respectively, and so can be considered negligible compared to local variability. A further lander was deployed in 2011, but was unfortunately lost, so the data set is presently limited to December 2011 but will be continued in future.

2.1.3. Ancillary Data Sets

In order to compare observations with regional surface forcing, we use the European Centre for Medium-Range Weather Forecasts (ECMWF) Interim Re-Analysis (ERAint hereafter) 6 h surface wind stresses,

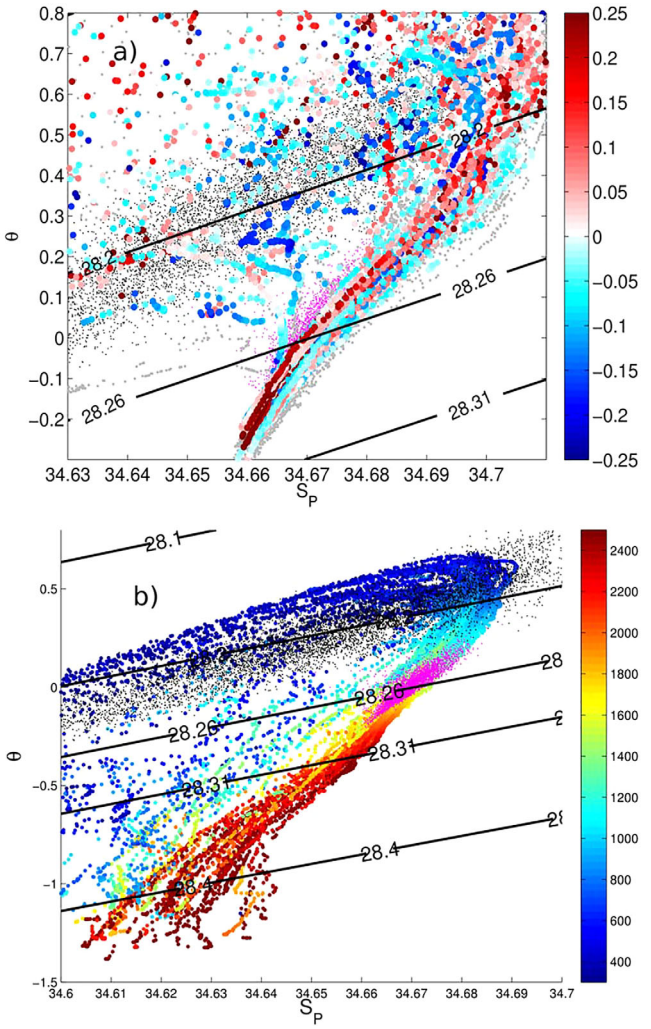

Figure 3. (a) Zonal velocity distribution of SR1b slope CTDs and bottom landers in potential temperature-salinity space. Positive values are m s^{-1} eastward, gray indicates no available velocity data. Small black dots indicate shallow bottom lander observations and maroon the deep bottom lander. (b) TS distribution from SR4 CTDs over the Weddell slope and shelf. Color indicates pressure (dbar), small dots indicate bottom lander observations as for Figure 3a. Neutral density contours are overlaid, note different axis positions.

averaged into monthly bins [*Dee et al*., 2011]. This data set was chosen for its accuracy at high latitudes [*Bracegirdle and Marshall*, 2012] and for compatibility with the model data set described below, which use it as a forcing field. The primary Southern Ocean modes of atmospheric variability, the Southern Annular Mode (SAM) and the El Niño Southern Oscillation (ENSO) are also compared with the hydrography. The monthly SAM index was obtained from the British Antarctic Survey (https://legacy.bas.ac.uk/met/gjma/sam.html) [*Marshall*, 2003] and the monthly Niño 3.4 index time series from the NOAA climate prediction centre (http://www.cpc.ncep.noaa.gov/data/indices/wksst8110.for). Finally, we examine the transport time scales between the Weddell Gyre and slope north of Elephant Island using the output of the eddy-permitting, data-assimilating Southern Ocean State Estimate (SOSE) [*Mazloff et al*., 2010]. This is done by advecting passive tracer in the daily mean model velocity fields, using the same model setup and tracer advection schemes described in *Wang et al*. [2014].

3. Results

3.1. Slope Current and TS Distribution

LADCP profiles are available for 13 occupations of the SR1b hydrographic section over the continental slope and show that for almost all of these years there is a westward flowing current over the continental slope between 1000 and 2500 dbar (Figure 2). In some years this is present in only a single profile, is less than 5 km wide, $<$10 cm s^{-1}, and does not reach the surface (e.g., 2001, 2002, and 2009). In other years the westward current extends over the full water column of the continental slope and shelf with velocities exceeding 25 cm s^{-1} (2000 and 2007). The instantaneous measured westward transport of these slope currents (south of 60.75°S) range from 0.1 to 5 Sv, with a mean of 1.5 $\pm$ 1.5 Sv westward. This agrees well with observations of between 1.4 and 3.2 Sv by *Nowlin and Zenk* [1988] but is less than the value of 5 Sv estimated at SR1b using an inverse model, although well within the range of uncertainty [*Naveira Garabato et al*., 2003]. It is also less than the 5–7 Sv of the Antarctic Slope Current observed immediately upstream at the South Scotia Ridge [*Heywood et al*., 2004]. Notably, this current is bottom-intensified and 0.9 $\pm$ 0.8 Sv of this westward transport occurs below 600 dbar. Figure 2 shows that the shallow and deep bottom lander positions are well placed to observe the westward slope transport.

The thermohaline characteristics of the westward slope current are distinct from the warm saline Circumpolar Deep water (CDW) found further offshore (or over the slope when no westward current is present), as well as the significantly fresher surface waters found on the shelf (Figure 3a). Over the continental slope

(i.e., depths between 600 and 2500 m) water with neutral densities around γ_n=28.2 kg m^{-3} and fresher than 34.68 S_P is dominantly westward flowing where LADCP data are available. The characteristics of westward flowing water on the SR1b section align with the spread of properties at the shallower bottom lander at 1000 dbar and further indicate that this instrument captures well the westward flowing current. The observations at 2000 dbar do not exhibit the same spread in TS space, but still tend to be cooler and fresher than SR1b observations of CDW at the same density. In between the deep and shallow bottom lander clusters are a number of CTD observations on the mixing lines between the two TS classes, suggesting that the slope current extends between the two depths. The TS characteristics observed at the bottom landers align closely with Modified Circumpolar Deep Water (MCDW) observed within the Weddell Sea over the continental slope on the SR4 section (Figure 3b). While the deep bottom lander TS distribution sits entirely within the SR4 observations at 1000–1500 dbar, the shallow bottom lander appears to be slightly cooler and fresher than water of the same density at SR4, while some is warmer and more saline. This may represent mixing with cooler and fresher shelf water and ACC CDW, respectively, during export from the Weddell to Scotia Sea [e.g., *Whitworth et al*., 1994].

The bottom properties observed by the bottom landers on the slope show that there is significant high-frequency variability in both temperature and salinity that is not resolved in the annual repeat SR1b hydrography (Figure 4). Despite this the broader agreement over the full SR1b time series with the smoothed bottom lander record is reasonable and agrees with the increase in temperature and salinity observed at the bottom lander (see discussion of long-term trends in section 3.3). At high frequencies, there are relatively short-lived spikes of cold, freshwater in the 1000 m record. Cold spikes have been observed previously in the temperature record at this location and were hypothesized the signature of shelf waters convecting downslope in the vicinity of Elephant Island [*Meredith et al*., 2004; *von Gyldenfeldt et al*., 2002]. The addition of salinity in the present observations show that these spikes are also fresh, supporting this hypothesis. It appears that these events feature water that is sufficiently dense to reach the 1000 m level, but not regularly to the 2000 m level. Because these events occur dominantly in the austral winter, a seasonal cycle in the temperature and salinity at the 1000 m level becomes apparent. This seasonality may be due to mixing of the convective spikes with ambient water [see *Su et al*., 2016a,2016b], advection of a seasonal signal from the Weddell Gyre, or some combination of both. This seasonal variability has been discussed previously [*Meredith et al*., 2004] and will make it difficult to infer meaningful dynamical relationships between the lander observations and other data sets that also include significant seasonal components (e.g., wind stress; see *Chelton* [1982] for a discussion of this problem). The presence of strong local seasonal forcing at the landers and possibly at other locations between the lander and the Weddell Gyre may also confound the analysis of teleconnections with remote forcing. Therefore, for the purpose of the present paper we remove the high-frequency convective spikes by averaging on monthly time scales and deseasonalize both the lander and surface forcing data sets. High-frequency events and the role of seasonality in driving variability at the landers will be discussed in a future analysis.

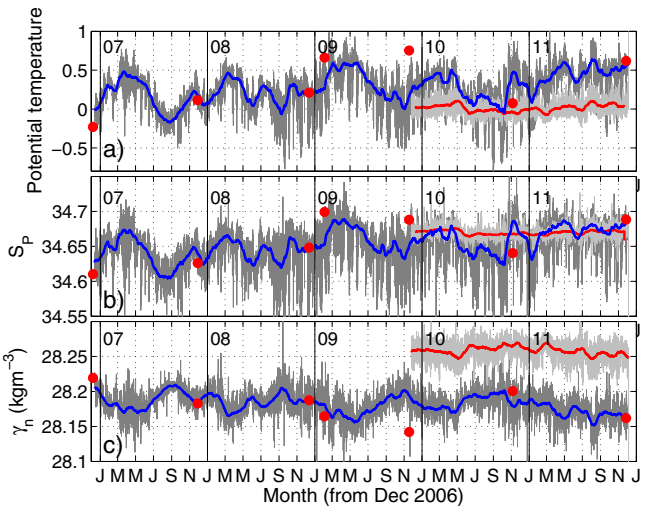

Figure 4. Bottom lander (a) potential temperature, (b) salinity, and (c) neutral density for (blue) shallow and (red) deep slope bottom landers. Gray lines indicates 15 min observations, while bold colored lines give the 2 week running mean. Red dots indicate the mean bottom 20 dbar properties from the nearest colocated CTD from SR1b. No CTD casts were conducted close enough to the deep bottom lander for meaningful comparison. Vertical black lines indicate the start of each calendar year.

3.2. Relationship of Slope Properties to Surface Forcing

Here we examine how the observed bottom properties at the bottom landers correlate with wider regional surface forcing. Several regional metrics were examined, including sea ice concentrations, sea surface height, sea level pressure, and zonal and meridional

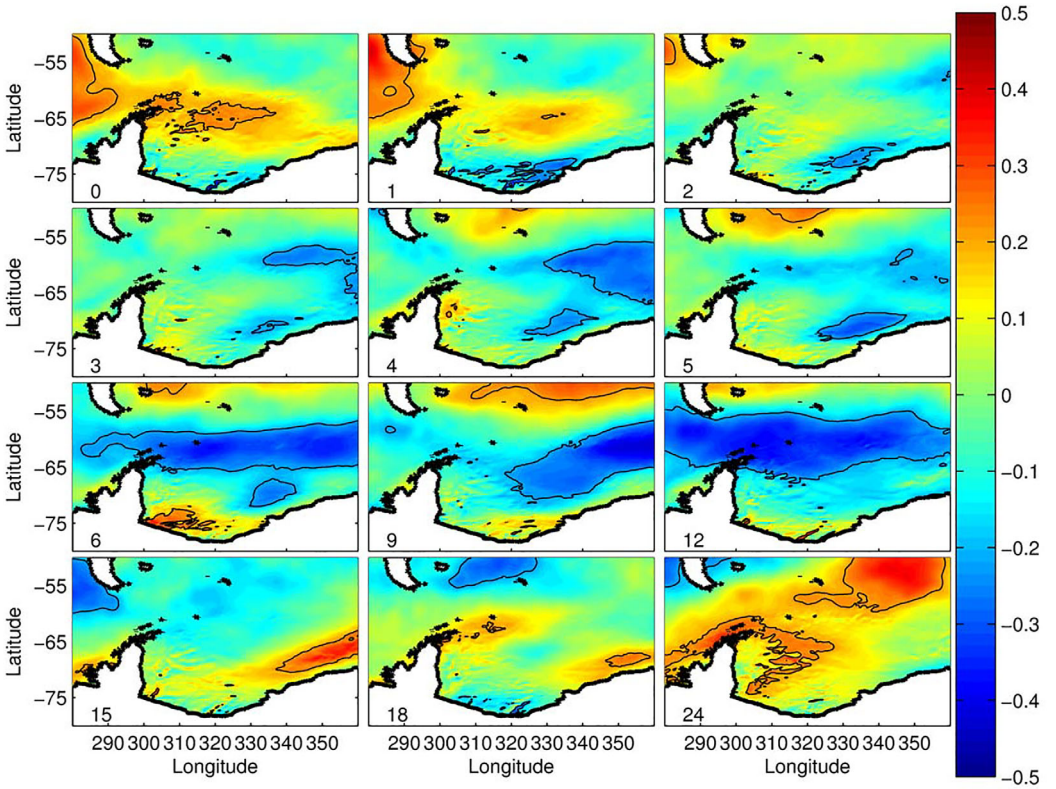

Figure 5. Correlation of shallow (1000 m) bottom lander density with eastward wind stress for lags of between 0 and 24 months (density lagging wind stress, labels) over the Weddell/Scotia region. Correlations are taken over the whole bottom lander record (2006–2011) and are made pointwise for deseasoned monthly means of both bottom lander and ERA-interim data. Similar correlations occur for weekly averaging, but are significantly spatially noisier. Fine lines indicate the edge of regions where correlation is significant at the 95% level.

wind stresses. The clearest relationships that emerged were with zonal wind stress, and these are discussed here. The lander neutral density (with similar results obtained for either potential temperature or practical salinity, not shown) was averaged into monthly bins to remove the influence of tides and short-lived spikes and the long-term linear trend was removed. The seasonal signal was then removed by subtracting the mean monthly property anomaly relative to the detrended series. This time series (from December 2006 to December 2011) was then correlated at lags between 0 and 24 months with the similarly deseasoned ERAint winds stress monthly anomalies at each point over the region. There is a weak positive correlation ($r < 0.25$) between bottom lander density and eastward wind stress in the immediate bottom lander region at zero lag (Figure 5). This suggests that it is possible that some signal may be related to changes in local conditions (e.g., isopycnal heave due to changes in wind stress or increased flow of dense water off the adjacent shelf) but this local correlation is weak compared with others in the region and explains less than 6% of lander density variance.

A more significant feature occurs at between 4 and 12 months lag where a clear (peaking at $|r| > 0.6$) and statistically significant negative correlation between lagged zonal wind stress and the bottom lander density emerges, with the strongest correlations centered over the South Scotia Sea and northern Weddell Sea at a lag of 6–12 months. This coherent relationship with the wind stresses over the wider Weddell Gyre suggests a dynamical link between wind forcing over the gyre and the properties of the water masses exported across the South Scotia Ridge and reaching the tip of the peninsula at around 1000 m depth.

As suggested by *Meredith et al*. [2008] one mechanism for such a link may be an increase in cyclonic (anticyclonic) wind stress curl increasing (decreasing) vertical Ekman pumping and spinning-up (down) the gyre. The point-by-point correlation of bottom lander density with wind stress curl is very noisy due to the derivative nature of wind stress curl (Figure 6). However, there are generally positive correlations to the south of 60°S in the wind stress curl versus density relationship, and negative correlations north of this. This is

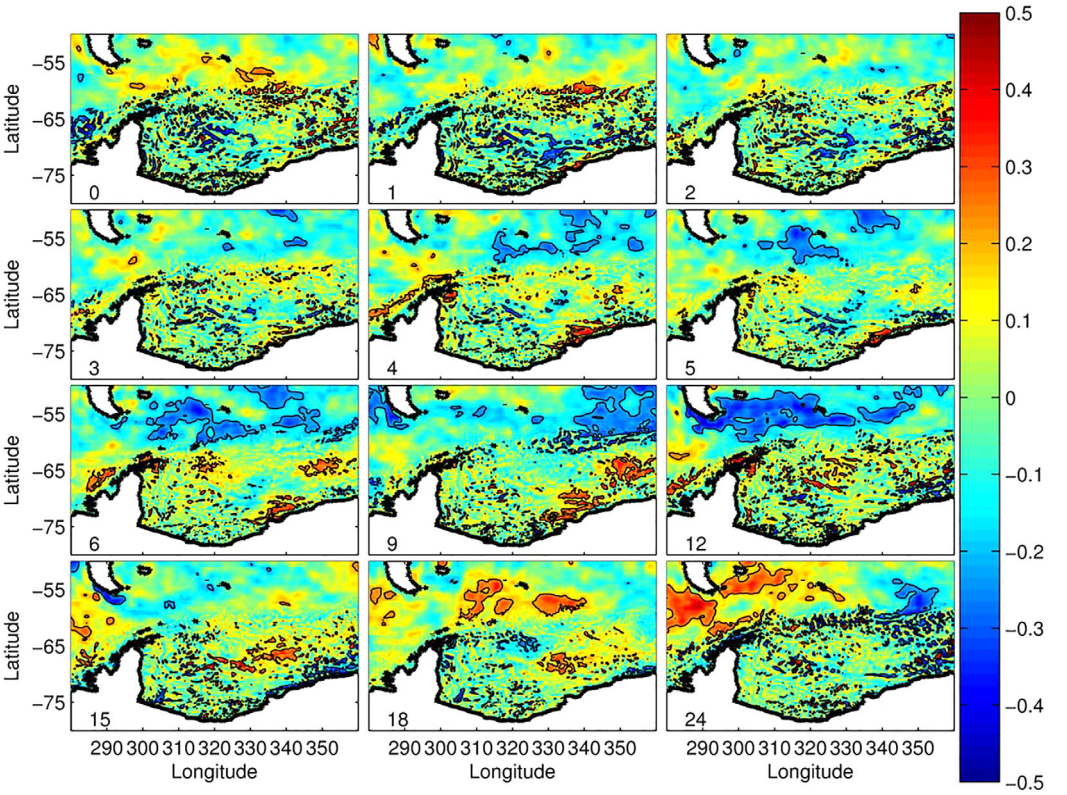

Figure 6. As for Figure 5 except this time correlating shallow bottom lander density with wind stress curl.

particularly pronounced at 4–12 months lag. This aligns with the region of negative correlation between density and zonal wind stress at the same lags and suggests that a decrease in the zonal winds at these latitudes is associated with a less cyclonic (i.e., less divergent) wind stress curl over the Weddell Gyre.

In order to examine this somewhat qualitative relationship in a more integrated sense, we average the wind stress curl over a number of regions within and over the whole gyre (see integration boxes in Figure 1). We find a significant positive correlation ($r > 0.4$) between the shallow (1000 m) bottom lander neutral density at 60°51.01′S, 54°42.64′W and wind stress curl over the whole gyre at lags of between 5 and 13 months (Figure 7a). This correlation is slightly stronger for wind stress curl integrated over the western part of the gyre ($r > 0.48$), but overall the same relationship emerges. This contrasts with the local wind stress curl integrated directly over the region of the bottom lander, where no statistically significant relation appears at any lag. A slightly more lagged pattern emerges for the deep instrument (peaking at 10–15 months), but at no time is it statistically significant, probably due to the shorter time series available for this instrument (Figure 7b). The slower response time at 2000 m relative to 1000 m may be due to longer transit times to reach the deep instrument (see section 4.3).

3.3. Relationship With Wind Stress Modes

The two primary modes of atmospheric variability over the Weddell Sea are the SAM and ENSO. We correlate the bottom lander potential density at 1000 m with these indices at lags between 0 and 24 months (Figure 8). As for other correlations performed in this analysis the SAM and ENSO monthly means were used and were deseasonalized. We find that the bottom lander density is significantly correlated with both the atmospheric indices at a lag of between 5 and 15 months, peaking at around 10–12 months lag with absolute R values between 0.45 and 0.55. The SAM and ENSO indices produce opposite correlations in their positive phases, with SAM being negatively correlated and ENSO (Ninõ 3.4) positively, with the density at the shallow bottom lander. This agrees with analysis in the previous section in that positive SAM phases generally act to produce stronger cyclonic wind stress curl over the Weddell gyre and spin it up [*Jullion et al.*,

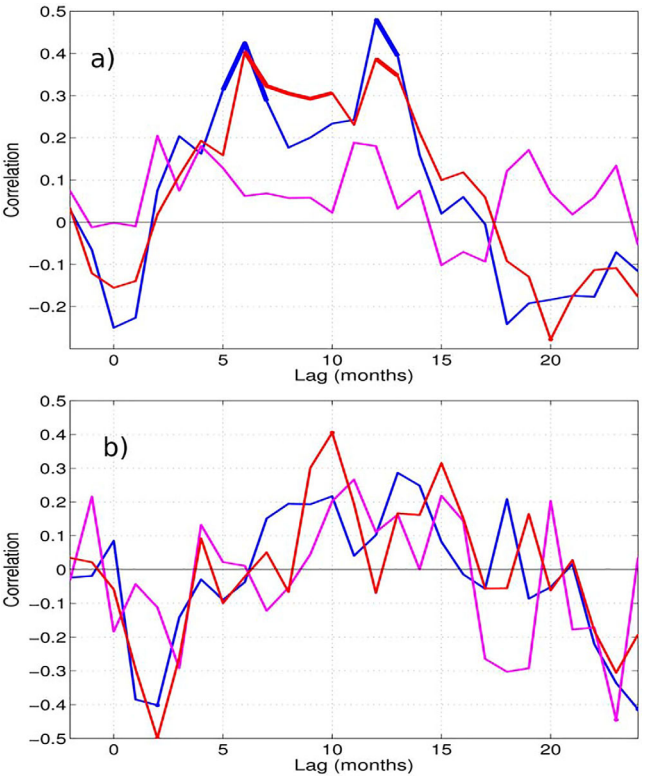

Figure 7. Correlation of (a) shallow (1000 m) and (b) deep (2000 m) bottom lander neutral density with wind stress curl at various lags between −2 and 24 months. Red corresponds to wind stress curl integrated over the whole gyre, blue over the western area and mauve over the bottom lander itself. See Figure 1 for integration regions. Correlations are calculated for detrended, season removed monthly means. Bold lines indicate a significant correlation at the 95% level.

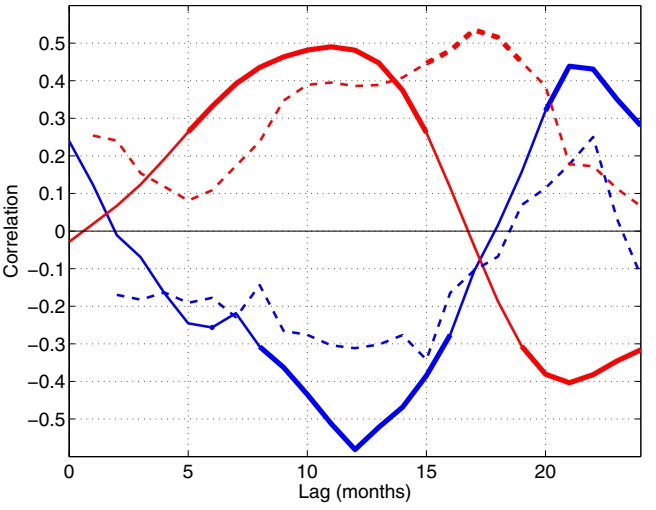

Figure 8. Lagged correlation between bottom lander neutral density monthly means at 1000 m and the SAM (blue solid line) and ENSO (red solid line) monthly indices between 2006 and 2011. This is contrasted with the correlation between the SR1b slope neutral density (see text) and the lagged SAM (blue dashed) and ENSO (red dashed) monthly indices. Bold lines indicate where the correlation is significant at the 95% confidence level.

2010], while El Ninõ events (positive in the Ninõ 3.4 index) are associated with the opposite effect. The SAM has the stronger correlation than ENSO with outflow from the Weddell Sea into the Scotia Sea, although ENSO is observed here to still exert a significant influence on outflow properties. This contrasts with *Jullion et al.* [2010] where ENSO was observed to be only weakly linked to the properties of WSDW property variability at SR1b.

We extend our examination over the full 21 year SR1b hydrographic time series over the slope, noting that such data cannot address the subannual variability in water mass properties we discuss above. The dashed lines in Figure 8 show the correlation between the mean slope neutral density (where the slope is defined as waters deeper than 600 dbar and south of 60.75°S) and the deseasonalized SAM and ENSO monthly indices sampled at the corresponding lag ahead of the hydrographic observations (Figure 9). Although only the ENSO index is significantly correlated with the slope properties at the 95% level, both the SAM and ENSO lag patterns agree qualitatively with the higher-frequency bottom lander analysis. The ENSO correlation coefficient reaches its maximum at 17 months, around 6 months later than the equivalent relation for the bottom landers. This difference may be due to either frequency-induced aliasing or by the generally deeper and possibly slower propagating signal sampled by the deeper slope average density than that sampled by the bottom lander at 1000 m.

There does not appear to be a long-term trend in the slope current properties over the SR1b observational period either in temperature, salinity, or transport/area of the westward current (Figures 10 and 11) although there is significant variability on interannual time scales. This variability includes a period of warming and salinification between 1995 and 2001, followed by cooling and freshening to a minimum in 2007,

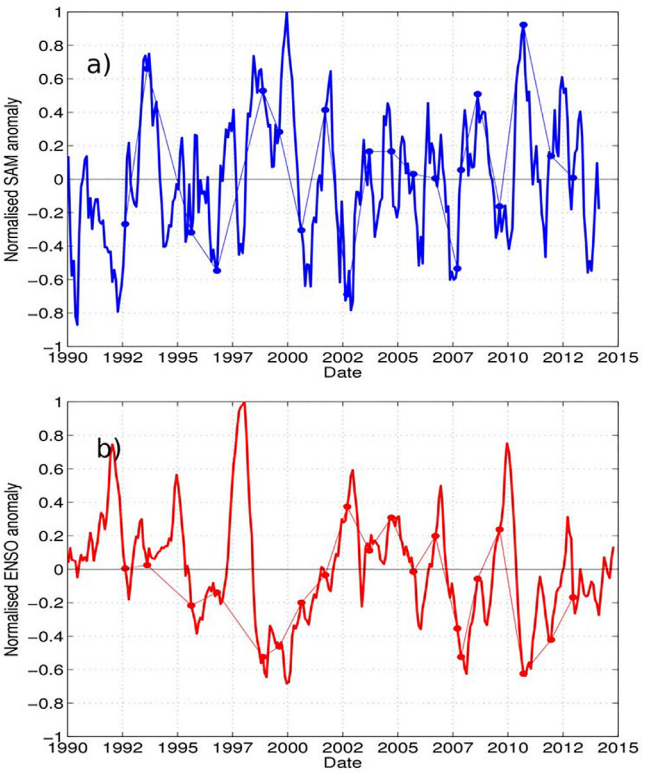

Figure 9. Time series of deseasonalized and normalized monthly (a) SAM and (b) ENSO atmospheric indices between 1990 and 2015 (bold lines). Fine lines and dots indicate the subsampling of these time series according to SR1b occupations, with a lag of 15 months where the correlation between atmospheric modes and slope current properties is greatest (see Figure 8).

and then warming and salinification again between 2007 and present. This final phase includes the bottom lander period (2007–2011) and shows its pronounced warming and salinification (Figure 4) to be part of a slower mode of variability. The cross-sectional area of the cold fresh slope current varies accordingly, and a maximum in observed cross-sectional area of $>20\pm7 \times 10^6$ m^2 occurs in 2007 in conjunction with the coldest and freshest observed mean slope values. There is a corresponding area minimum in 2001. Here cross-sectional area is calculated based on interpolated CTD observations with potential temperatures $<0.3^\circ$C and $S_P < 34.68$ below 600 dbar and south of 60.75°S. These values were chosen as a conservative estimate of characteristics falling within the westward flowing regime (Figure 3). Error estimates are calculated using 1000 Monte Carlo iterations where the defining temperature, salinity, and northern boundaries are varied by up to ±10%. LADCP observations of westward transport are only sporadically available during the time series so it is difficult to assess the transport variability of the slope current (Figure 11). However, qualitatively they do appear to covary with the cross-sectional area of the cold/fresh slope current, being at a maxima of 1.7 ± 0.45 Sv around 2008 and a minima of less than 0.10 ± 0.05 Sv in 2002 and 2009. To the extent that this relationship holds more generally, this suggests that the cross-sectional area of the current dominates the transport, rather than the export velocity. Figure 11 suggests that both cross-sectional area and transport of the slope current may be increasing slightly with time, though such a trend is not statistically significant with the present length of record.

4. Discussion

4.1. Antarctic Slope Current Extension

The clear alignment between the TS properties observed in the cool fresh slope current on the slope north of Elephant Island and the properties over the slope within the Weddell Sea at SR4 (Figure 3b) support the hypothesis of *Nowlin and Zenk* [1988] and *Garabato et al.* [2002] that a significant contributor to the westward flow at SR1b is Weddell Sea waters. The agreement between the SR4 slope properties and those observed at the bottom landers leads us to hypothesize that this westward flowing core represents an extension of the ASC, which has exited the Weddell Sea following isobaths and passing through the various sills of the South Scotia Ridge west of Orkney Plateau. *Heywood et al.* [2004] observe the ASC moving eastward with a transport of approximately 7 Sv on the northern boundary of the Hesperides Trough immediately south east of Elephant Island, but do not observe it on the northern side of the South Scotia Ridge in the vicinity of Philip Passage (48°W). They theorize that the ASC loses its characteristics here via mixing eastward with ambient CDW. *Palmer et al.* [2012], however, find a similar export value of 7 ± 4 Sv of water $28.1 < \gamma_n < 28.27$ kg m^{-3} entering the Scotia Sea via several sills in the northern boundary of Hesperides Trough, significantly west of Philip Passage. Notably they observe around 1.58 ± 1.1 Sv exiting into the Scotia Sea in jets with velocities over 0.2 m s^{-1} in depth ranges between 600 and 1600 m at gaps at 52.5°W

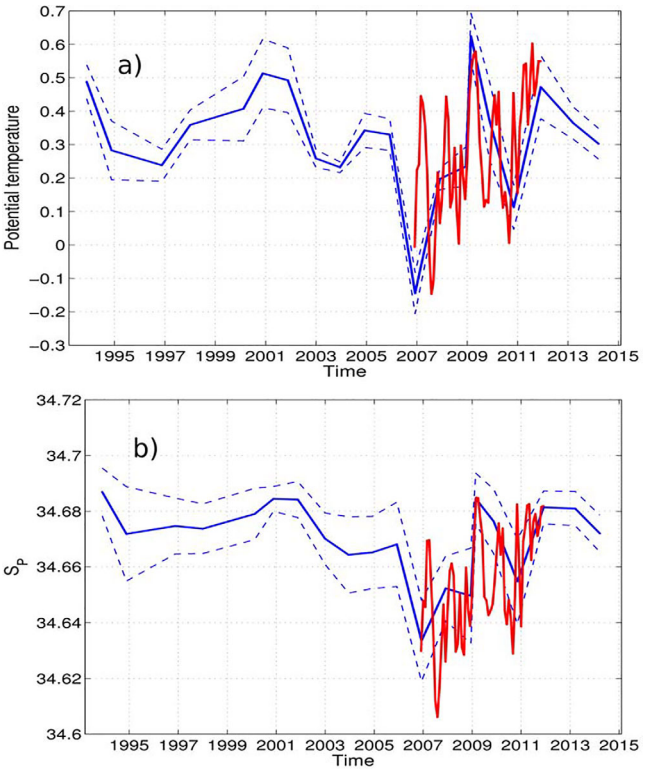

Figure 10. Bottom lander monthly mean (a) potential temperature and (b) salinity (red line), compared with equivalent SR1b mean slope properties. Here slope is defined as below 600 dbar and south of 60.75°S. Dashed lines indicate two standard deviations in slope properties based on 1000 Monte Carlo iterations for various definitions of the slope current (see text for details).

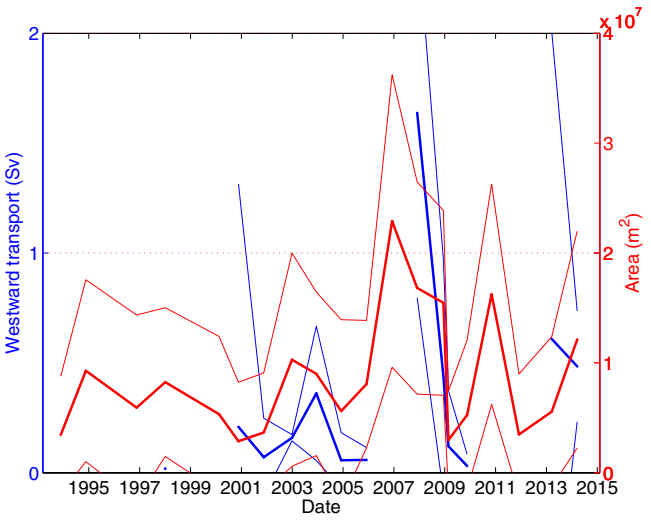

Figure 11. Time series of westward slope current cross-sectional area (red) and (where available) westward volume transport (blue) over the continental slope during SR1b occupations. Fine lines give two standard deviations based on 1000 Monte Carlo iterations for various definitions of the slope current (see text for details).

and 51°W (1000 m isobath in Figure 1b), and associate these pathways with a branch of the ASC. This transport value aligns well with the 1.5 ± 1.5 Sv estimated at SR1b in this study. Along with the narrow westward jet and velocities of over 0.25 m s^{-1} at the shelf break we suggest that this indicates that a limb of the ASC extends, at least intermittently, along the northern boundary of the South Scotia Ridge as far west as Elephant Island, and likely beyond.

The water over the slope within the Weddell Sea at SR4 with thermohaline characteristics matching the SR1b bottom landers is found to be around 500 dbar shallower than at their respective bottom lander sites (Figure 4). This suggests that upon crossing the Scotia Ridge at between 600 and 1600 m as observed by *Palmer et al.* [2012] and encountering less dense ambient ACC water this Weddell Sea water descends down the continental slope, turning with Coriolis as it does so and forming a westward flowing current along the continental slope.

4.2. Slope Properties and Variability Over the Wider Scotia Sea

The longer-term (decadal) changes we observe over the slope north of Elephant Island agree with wider changes in LCDW of similar densities integrated over the rest of the SR1b section. We define slope here as south of 60.75°S and below 600 dbar, while LCDW is taken to be all water with $28.00 < \gamma_n < 28.26$ kg m^{-3} and north of 60.75°S. We observe no significant change in LCDW salinity between 1997 and 2002, followed by a reduction in mean salinity of 0.017 ± 0.003 S_P to 2007–2009 and then an increase again of 0.010 ± 0.003 S_P to present (Figure 12). This agrees closely with a similar analysis in *Jullion et al.* [2013]. The timing of these changes in LCDW align well with the changes over the slope observed in the present study ($r > 0.65$, $p < 0.002$), though the magnitudes of change in the mean slope salinity (up to 0.050 ± 0.012 S_P between 2001 and 2007) are

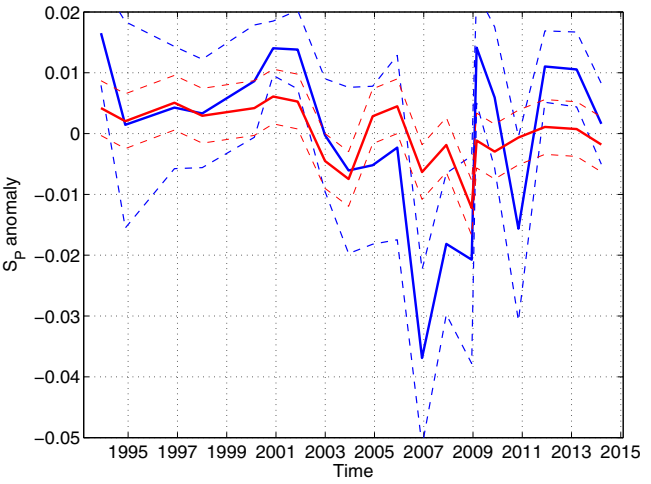

Figure 12. Time series of mean SR1b (blue) slope and (red) LCDW salinity anomalies. Slope properties are defined as below 600 dbar and south of 60.75°S while LCDW is defined as in [*Jullion et al.*, 2013] as 28.00 $< \gamma_n <$ 28.26 kg m^{-3} and north of 60.75°S. Error bars for slope properties give two standard deviations calculated based on 1000 Monte Carlo iterations for various definitions of the slope current and errors. Error bars for LCDW are based on errors calculated in *Jullion et al.* [2013].

several times larger than that of waters of similar density averaged over the whole SR1b section. This suggests that the changes over the whole section are driven by the same export of Weddell Sea water and that the changes are most pronounced over the slope as they are closest to the source waters.

The long-term variability in exported Weddell Sea water north of Elephant Island reported here also agrees with observations of Warm Deep Water (WDW; a CDW class exported from within the Weddell Gyre, with $\gamma_n <$ 28.2 kg m^{-3}) found in the Eastern Scotia Sea. *Meredith et al.* [2008] observe that south of the Southern Boundary of the ACC at the A23 section (around 31°W) WDW warmed and became more saline between 1995 and 1999, and then cooled and freshened to 2005. Although a sparse time series, the broad sense of these changes are consistent with our observations in the western Scotia Sea at SR1b. Notably, much of the WDW in the eastern Scotia Sea is likely to have been exported over the South Scotia Ridge east of Orkney Plateau while the water on the slope north of Elephant Island is likely to have been exported west of Orkney Plateau. The agreement in interannual variability and timing between the two regions suggests a common driver via changes in the volume or properties of the outflow of Weddell Sea waters.

No significant trend in either slope water or LCDW properties over the whole SR1b emerges in Figures 4 or 12. Given their correlation with SAM and ENSO this agrees well with the negligible trends in these two atmospheric indices between 1993 and present (Figure 9). However, not all export trends observed in the Scotia Sea agree with those observed on the slope at SR1b. The densest water masses on SR1b, the LWSDW with $\gamma_n >$28.31 kg m^{-3} consistently freshened over the whole section time series from 1993 onward [*Jullion et al.*, 2013], and do not display the same variability in response to changes in wind forcing. This supports the argument in *Jullion et al.* [2013] that this trend is due to changes in the source water masses and formation characteristics of shelf and bottom water within the Weddell Sea rather than predominantly volume export variability.

4.3. Export Response Time Scales

Variability of the Scotia Sea water masses described above has also been linked to changes in the SAM mode and surface wind stress. For example, *Jullion et al.* [2010] find that during positive SAM phases (stronger cyclonic wind stress over the gyre) warmer and more saline WSDW is exported from the Weddell Gyre to the Scotia Sea and WSDW density on the SR1b line is reduced. They find a 5 month lag between SAM anomalies and response on the SR1b section, slightly faster than the 8–16 months observed in this study. This difference may be due to the sparser SR1b time series available to the earlier study or different response times of the deep versus slope water masses.

To further explore the time scale of the response between changes in the wind stress curl and properties observed on the SR1b section, we examine whether changes on the north-west Weddell sea slope may be transmitted to the bottom lander sites within the 6–13 months indicated by the correlations in Figures 5 and 7. Figure 13 shows the concentration of a modeled passive tracer released within the SOSE model over the continental shelf and slope at 64°S, close to the SR4 line. Three tracers were released, an upper tracer over the shelf at 0–440 m, intermediate over the continental slope between 500 and 2300 m and deep at ranges between 2600 and 3300 m. Four instances of each release were run with tracer being released at

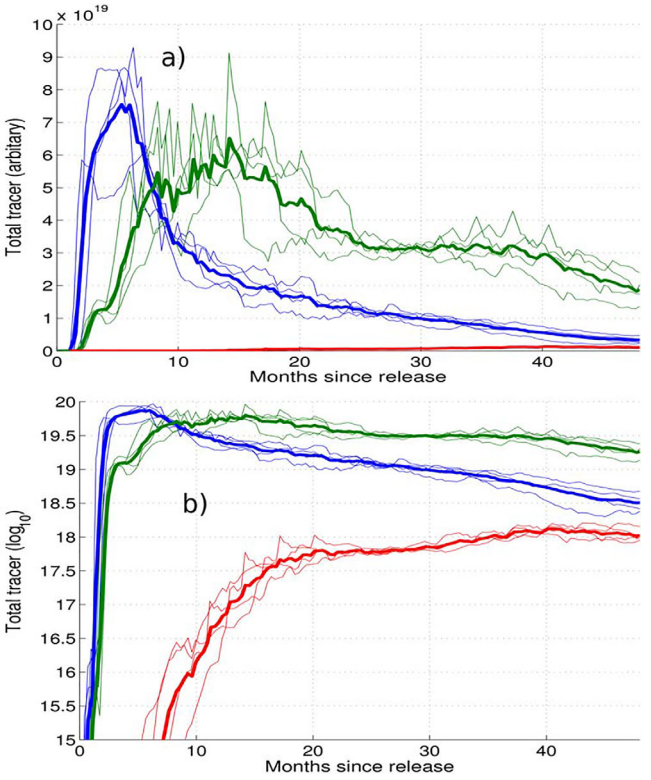

Figure 13. Time series of SOSE modeled total passive tracer concentration at the SR1b section after release in the Weddell Sea on (a) linear and (b) logarithmic *y* axis. Three tracers were released over the continental slope near the SR4 section at depths of 0–500 m (blue), 500–2000 m (green), and 2000–4000 m (red). Fine lines show each instance of the tracer release, and bold lines give the mean for each release depth across all instances (see text for details).

each depth range on the first of January, April, July, and October of modeled year 2006. The shallowest tracer reaches the SR1b section first within 3 months, with the concentration peaking at around 6 months. The intermediate-depth (slope) tracer appears around the same time, but peaks between 8 and 14 months. The deep tracer does not register at SR1b except in very small concentrations, around 2 orders of magnitude smaller than the upper or middle tracer and after between 10 and 20 months. This spread is largely because the deep tracer must transit to the Scotia sea via the Orkney Passage and is mostly dispersed eastward, the shallow tracer flows directly over the shelf and the intermediate tracer follows isobaths to exit the Weddell Sea via the sills west of Orkney Plateau as suggested in section 4.1.

The intermediate-depth pathway is most representative of the depth range of the bottom landers, so we examine it in more detail. Figure 14 shows the column integrated intermediate tracer density over the first 3 years of the release experiment, along with a pathway following the tracer peak west of Orkney Plateau from release site to lander location. A Hövmoller diagram of the spread of tracer along this pathway shows that the vertically integrated tracer flows in a fairly coherent mass along the continental slope in the ASC at a velocity of approximately 0.07 m s^{-1} to the bifurcation point (B in Figure 14) south of Philip Passage (Figure 15). At this point the column-integrated tracer velocity drops to about 0.04 m s^{-1} and the tracer is distributed more unevenly along the path with time. This spread is due to the tracer following alternative paths and recirculations as it crosses the South Scotia Ridge, but a concentration peak is still evident, reaching the north side of the South Scotia Ridge (C in Figure 14) and the lander positions near 1100 km along the tracer path at approximately 9–10 months for the January and April releases, and between 10 and 12 months for July and October releases. The average velocity directed along this pathway is 0.059 ± 0.025 m s^{-1} at 1000 m, and 0.040 ± 0.028 m s^{-1} at 2000 m, with the mean velocity being around 20% faster in the Weddell Sea sector south of the bifurcation point. This velocity varies by season, with modeled surface velocities peak at over 0.07 m s^{-1} in April–May and are at a minimum of around 0.04 m s^{-1} in October. These values are on the low side for the ASC where mean surface velocities of up to 0.2 m s^{-1} have been estimated [*Youngs et al*., 2015; *Palmer et al*., 2012] and flow at depth over the sills of the South Scotia Ridge have mean velocities of 0.08 m s^{-1} [*Nowlin and Zenk*, 1988]. This slower modeled velocity may be due to the difficulty in resolving the sharp ASC in the 1/6° resolution SOSE, but still provide a useful bound on gyre response times.

Notably, the intermediate tracer arriving first at the landers does not follow the Philip Passage pathway tracer peak in Figure 15, but instead appears on the pathway at around 1000 km (point C) before flowing to the lander location. Based in Figure 14 this tracer appears to take a faster pathway through gaps in the North Scotia Ridge west of Philip Passage and is responsible for the rapid rise in intermediate tracer concentration between 5 and 8 months in Figure 13. Following this the bulk of the tracer flowing through Philip Passage reaches the landers and drives the tracer concentration peak in months 8–14. The presence of multiple

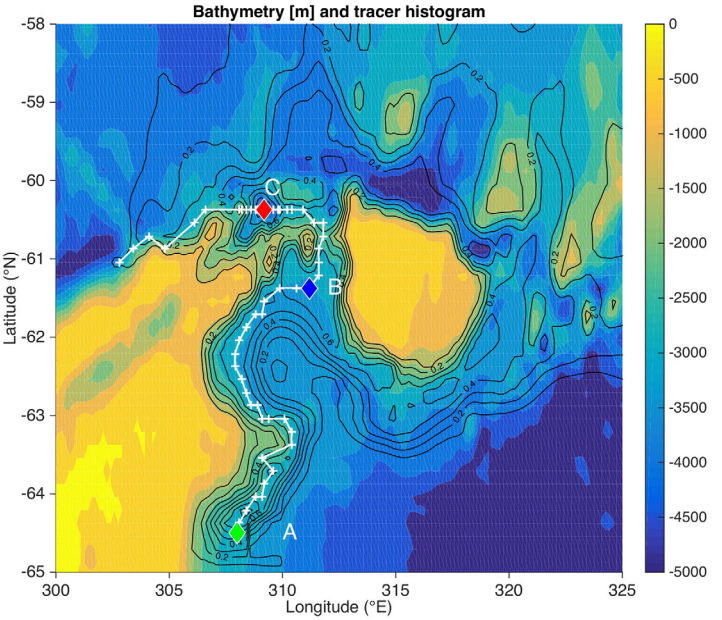

Figure 14. Column-integrated histogram of the tracer released in April 2006 (solid black lines) and model bathymetry (color). The histogram is scaled by its maximum value over the three-year experiment. The most direct path is indicated by a white line and white crosses. Also shown is the tracer initialization site (A, green diamond), bifurcation point (B, blue diamond), and the reference point on the north side of the South Scotia Ridge (C, red diamond).

pathways and seasonal velocity variations means that the exact transit time is difficult to determine. This spread may also explain the presences of the broad peak in lagged correlation in Figure 7, with the two distinct, statistically significant peaks at 6 and 12 months possibly representing the presence of two distinct pathways for telecommunication between the gyre and lander position. However, the comparatively low resolution of SOSE and its marginal representation of the complicated bathymetry of the South Scotia Ridge means this conclusion is hypothetical only.

Assuming SOSE represents an under estimate of transit time and using the *Nowlin and Zenk* [1988] slope mean velocity of 0.08 m s^{-1} (corresponding to a transit time of 5 months and the first appearance of significant amounts of intermediate tracer at the lander) and the middle of the observed density/wind stress curl correlation peak at nine-ten months in Figure 7 we arrive at a lag of 4–5 months between wind stress curl change and ASC response within the gyre. This agrees with the 5 month lag between changes in wind stress curl and an eddy modulated response of the ASC in the north west Weddell Sea estimated in observations [*Youngs et al.*, 2015] and idealized models [*Su et al.*, 2014]. If we instead use the modeled tracer transit time of 10 months to peak concentration, we find practically zero lag between wind stress changes and gyre response. This implies that a 5 month lag between changes in wind and gyre response may represent an upper limit, and thus not precluding at least a role for more rapid barotropic ASC responses to changes in wind stress curl. This obviously comes with the caveat that SOSE likely under-represent export velocities.

This tracer analysis also sheds light on the difference in lags for peak correlations between integrated wind stress curl and density by depth seen in Figure 7. The observed peak correlations occur approximately 4 months later at the deep lander than the shallow lander. The difference in SOSE current velocities along the peak tracer concentration pathway between 1000 and 2000 dbar is approximately 0.02 m s^{-1}. Over the 1200 km path length this difference translates to approximately 4 months difference in transit time, suggesting that baroclinic shear may be the cause of the observed differences in response times with depth at the lander position.

4.4. Dynamics Driving Weddell Sea Export Variability

As discussed in section 1 several dynamical explanations for the mechanism of gyre export response to changes in wind stress curl have been advanced. *Meredith et al.* [2011] postulate a barotropic acceleration of the ASC may drive a downslope bottom Ekman transport, deepening the isopycnal intersection with the South Scotia Ridge in the regions where the ASC flows through the ridge sills and thus changing the properties of the water escaping above the sill. Over the southern continental slope of the South Scotia Ridge they estimate that changes in barotropic velocity of the order of 0.05 m s^{-1} are enough to change the downslope component of Ekman transport sufficiently to produce vertical isopycnal displacements of hundreds of meters.

Su et al. [2014] propose an alternative explanation whereby mesoscale eddies act on the gyre isopycnal tilt imposed by changes in wind stress curl and act to rapidly propagate these changes in isopycnal depth to the gyre boundaries. In an idealized model they find that isopycnal depths at the gyre boundary respond to

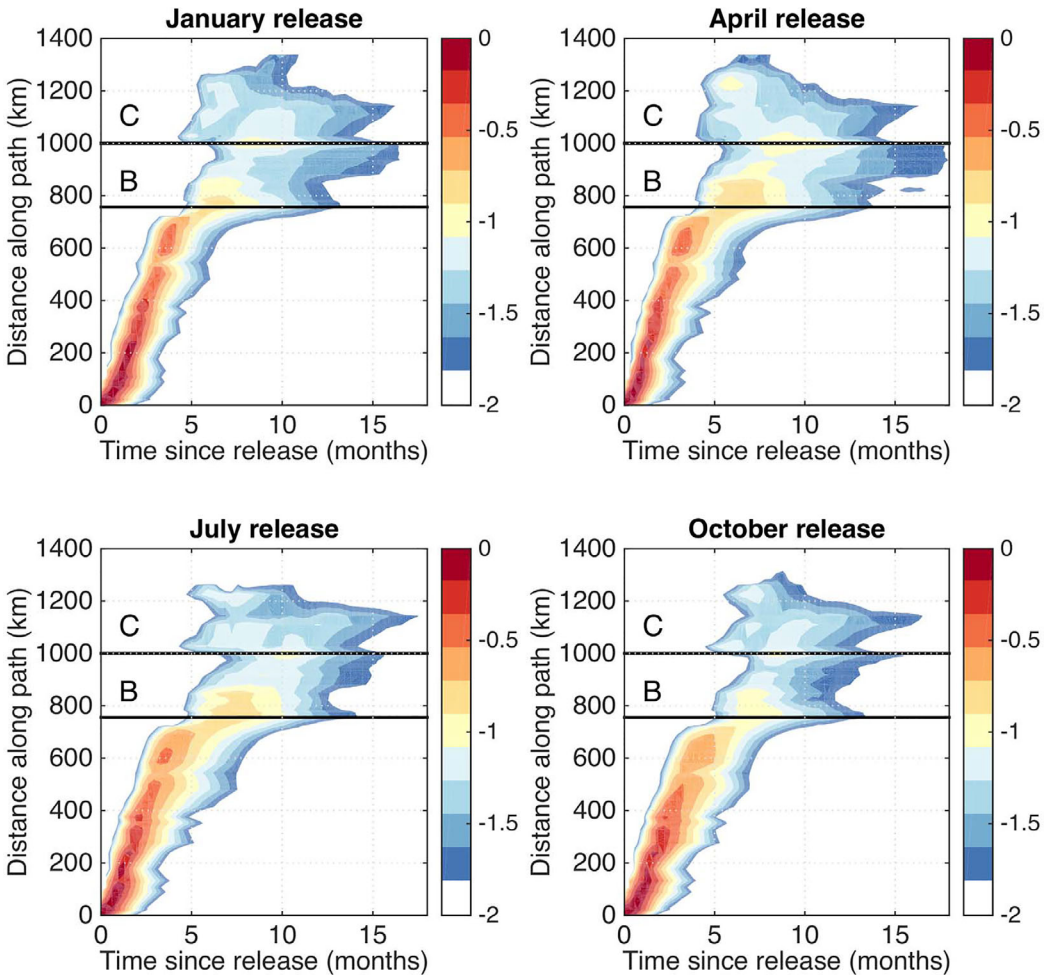

Figure 15. Hovmöller diagrams for the four seasonal tracer release experiments. The distance is along the pathway shown in Figure 14. The column-integrated tracer inventories (color, log10 scale) are shown relative to the maximum value along the pathway. Also shown are the positions of reference points B and C as indicated in Figure 14.

changes in wind stress curl via eddy propagation on the order of 5 months. *Thompson et al*. [2014] infer the presence of such mesoscale eddies in observations near the SR4 section and suggest such cross-ASC transport may support the enhanced bottom Ekman transport associated with an increase in ASC transport in response to a barotropic gyre spin-up. In a study of drifter releases near the SR4 section *Youngs et al*. [2015] find that in release years with strongly cyclonic wind stress curl the ASC moves further offshore (deepening isopycnals) and accelerates, while its surface temperature increases by around 0.5°C. They associate an increase in surface temperature in the ASC with a reduction in cross-frontal mixing of cold fresh shelf waters due to the enhanced PV barrier imposed by the accelerated mean flow.

Without a good time series covering the vertical extent of the ASC within the Weddell gyre, and with an estimated horizontal resolution of 1 km required for accurate eddy modeling [*Thompson et al*., 2014], it is difficult to discern which of the above hypotheses can most readily explain the variability we observe. However, there is some evidence to suggest that cross-frontal mixing may be associated with ASC strength. Figure 4b shows that the thermohaline properties observed at the shallow bottom lander broadly agrees with the range of MCDW around $\gamma_n = 28.2$ kg m^{-3} observed at 500–1000 dbar on the SR4 slope within the Weddell gyre. However, at some times it is considerably cooler and fresher than the Weddell gyre water of the same density (associated with a reduction of cyclonic forcing in section 3.2), while at others it is warmer and more saline (an increase in cyclonic wind stress curl). This may suggest that when the cyclonic forcing is strong cross-frontal mixing of cool fresh shelf water is reduced due to a stronger ASC and a greater PV barrier, resulting in warmer more saline export across the South Scotia Ridge; while when the cyclonic wind stress is weaker more cross-frontal eddy mixing occurs and cooler, fresher water is exported. This does not

preclude the role of bottom Ekman transport in setting isopycnal slope in response to a barotropic gyre spin-up, but does at least qualitatively suggest that cross-frontal transport by mesoscale eddies may be an important factor in setting the outflow characteristics of the ASC and Weddell Gyre west of Orkney Plateau.

5. Conclusions

We examine shipboard CTD data from the Drake Passage hydrographic repeat section between 1993 and 2014, as well as high temporal resolution data from two bottom landers deployed on the Antarctic continental slope between 2006 and 2011. We demonstrate the presence of a westward flowing slope current, observed between 500 and 2500 dbar over the continental slope north of Elephant Island on the tip of the Antarctic Peninsula. The slope current is bottom intensified, transports an average of 1.5 $\pm$ 1.5 Sv and is present in most occupations between 1993 and 2014. This current is significantly cooler and fresher than the ambient CDW found further offshore at similar densities (γ_n = 28.20–28.26 $\pm$ 0.05 kg m^{-3}) and has thermohaline characteristics closely aligned with Weddell Sea water found between 500 and 1000 dbar over the continental slope in the north west Weddell Sea. We hypothesize that the slope current at Elephant Island represents an extension of the Antarctic Slope Current, after it has crossed the South Scotia Ridge following isobaths through sills >1000 m deep west of 49°W. This pathway represents approximately a seventh of the total export of WDW from the Weddell Sea to the Scotia Sea west of Orkney Plateau [*Palmer et al*., 2012], and a 10th of the total transport of WDW across the South Scotia Ridge [*Naveira Garabato et al*., 2003]. It also shows that at least a portion of the ASC survives north of the South Scotia Ridge, rather than being completely mixed away in the Weddell-Scotia Confluence as suggested by *Heywood et al*. [2004]. The degree to which the ASC remains coherent and identifiable as such west of the SR1b section is unclear at present, but may penetrate as far as 64°W [*Garabato et al*., 2002].

The properties of the slope current exhibit significant variability on seasonal and interannual time scales, and we show that they are strongly and significantly correlated with changes in the wind stress curl integrated over the Weddell Gyre. This wind stress curl correlation with slope densities north of Elephant Island peaks at lags between 6 and 13 months after changes in the wind. This relationship exists in both the 5 year high-resolution bottom lander time series and the twenty 1 year annual occupation of SR1b, suggesting that it is a robust feature on multiannual time scales. The relationship between properties and change in wind stress curl, as well as the observed lag, is consistent with that seen in other studies for variability in deeper Scotia Sea water masses, such as WSDW integrated over the whole SR1b section, but also the eastern Scotia Sea at A23. This suggests that export from the Weddell to Scotia Sea through the sills both to the east and west of the Orkney Plateau responds to a common regional mechanism. The most likely candidate for this is a coherent change in the strength of the Weddell Gyre, either via baroclinic modification of the isopycnal doming over the whole gyre or barotropic acceleration of the boundary current. Given the rapidity with which the export responds to changes in wind stress, it seems more likely to be the latter, but without observations within the gyre itself it is difficult to be sure of the exact mechanism that relates warmer, more saline (colder, fresher) export to an increase (decrease) in wind stress cyclonicity over the gyre. The time scale of gyre slope current response to wind stress curl changes of around 5 months agrees with the response times modeled in *Su et al*. [2014] and observed in surface drifters in *Youngs et al*. [2015]. However, we note that this may represent an upper limit, thus not precluding a role for barotropic ASC acceleration. We also find circumstantial evidence to suggest that during periods of strong (weak) ASC flow mixing of cold fresh shelf water across the ASC within the western Weddelly Gyre may be suppressed (enhanced), lending credence to the suggestion by *Thompson et al*. [2014] that cross-slope mixing by mesoscale eddies may be regionally important for balancing downslope Ekman transport and setting ASC properties.

Regardless of the mechanism, the broad coherence of interannual variability between the slope current observed north of Elephant Island and the properties of large water masses over the whole SR1b [*Jullion et al*., 2010] and southern A23 sections [*Meredith et al*., 2011] indicate that changes in atmospherically forced Weddell Sea export is a key driver of Scotia Sea variability. We find no significant trend in the outflow properties and that wind driven variability contributes significantly to the temporal signal of both the slope current and LCDW. Further examination of the mechanisms of gyre export are required in order to understand how future changes in wind stress may influence Weddell Sea export, and in particular there is a clear need for long-term observations of the ASC within the gyre itself to address this dynamical linkage.

Acknowledgments
We would like to thank the many (many!) scientists, technicians, officers, and crews of the vessels who made the observations constituting the SR1b and SR4 sections. We would also like to thank Matthew Mazloff for providing the SOSE data and his support and encouragement in the use of it. Computational resources for the SOSE were provided by NSF XSEDE resource grant OCE130007. The lander data were obtained through the Natural Environment Research Council (NERC) National Capability Project ACCLAIM (Antarctic Circumpolar Current Levels by Altimetry and Island Measurements), which is supported by the Remote Sea Level Group at the National Oceanographic Centre. A.C.N.G. supported partially by NERC via the ANDREX project (NE/E01366X/1 and NE/E013368/1). D. C. Jones supported partially by NERC via the EXPOSE project (NE/J008494/1). The statements, findings, conclusions, and recommendations are those of the authors and do not necessarily reflect the views of NERC. All data used in this study are publicly available either through the British Oceanographic Data Centre, SOSE website (http://sose.ucsd.edu/) or through direct correspondence with the corresponding author (andmei@bas.ac.uk).

References

Anderson, D. L., and A. Gill (1975), Spin-up of a stratified ocean, with applications to upwelling, *Deep Sea Res. Oceanogr. Abstr.*, *22*, 583–596.
Bracegirdle, T. J., and G. J. Marshall (2012), The reliability of Antarctic tropospheric pressure and temperature in the latest global reanalyses, *J. Clim.*, *25*(20), 7138–7146.
Chelton, D. B. (1982), Statistical reliability and the seasonal cycle: Comments on "Bottom pressure measurements across the Antarctic Circumpolar Current and their relation to the wind," *Deep Sea Res., Part A*, *29*, 1381–1388.
Dee, D., et al. (2011), The ERA-Interim reanalysis: Configuration and performance of the data assimilation system, *Q. J. R. Meteorol. Soc.*, *137*(656), 553–597.
Fahrbach, E., M. Hoppema, G. Rohardt, M. Schröder, and A. Wisotzki (2004), Decadal-scale variations of water mass properties in the deep Weddell Sea, *Ocean Dyn.*, *54*(1), 77–91.
Garabato, A. C. N., E. L. McDonagh, D. P. Stevens, K. J. Heywood, and R. J. Sanders (2002), On the export of Antarctic bottom water from the Weddell Sea, *Deep Sea Res., Part II*, *49*(21), 4715–4742.
Gordon, A. L., M. Visbeck, and B. Huber (2001), Export of Weddell Sea deep and bottom water, *J. Geophys. Res.*, *106*(C5), 9005–9017.
Heywood, K. J., A. C. Naveira Garabato, D. P. Stevens, and R. D. Muench (2004), On the fate of the Antarctic Slope Front and the origin of the Weddell Front, *J. Geophys. Res.*, *109*, C06021, doi:10.1029/2003JC002053.
Jullion, L., S. Jones, A. Naveira Garabato, and M. Meredith (2010), Wind-controlled export of Antarctic Bottom Water from the Weddell Sea, *Geophys. Res. Lett.*, *37*, L09609, doi:10.1029/2010GL042822.
Jullion, L., A. C. Naveira Garabato, M. P. Meredith, P. R. Holland, P. Courtois, and B. A. King (2013), Decadal freshening of the Antarctic Bottom Water exported from the Weddell Sea, *J. Clim.*, *26*(20), 8111–8125.
Marshall, G. (2003), Trend in the southern annular mode from observations and reanalyses, *J. Clim.*, *16*, 4134–4143.
Marshall, J., and K. Speer (2012), Closure of the meridional overturning circulation through Southern Ocean upwelling, *Nat. Geosci.*, *5*, 171–180.
Martinson, D. G., and R. A. Iannuzzi (2003), Spatial/temporal patterns in Weddell gyre characteristics and their relationship to global climate, *J. Geophys. Res.*, *108*(C4), 8083, doi:10.1029/2000JC000538.
Mazloff, M. R., P. Heimbach, and C. Wunsch (2010), An eddy-permitting Southern Ocean state estimate, *J. Phys. Oceanogr.*, *40*(5), 880–899.
Meijers, A. (2014), The Southern Ocean in the Coupled Model Intercomparison Project phase 5, *Philos. Trans. R. Soc. A*, *372*(2019), 20130296.
Meredith, M., P. Woodworth, C. Hughes, and V. Stepanov (2004), Changes in the ocean transport through Drake Passage during the 1980s and 1990s, forced by changes in the Southern Annular Mode, *Geophys. Res. Lett.*, *31*, L21305, doi:10.1029/2004GL021169.
Meredith, M., A. Garabato, A. Gordon, and G. Johnson (2008), Evolution of the deep and bottom waters of the Scotia Sea, Southern Ocean, during 1995-2005, *J. Clim.*, *21*, 3327–3343.
Meredith, M. P., A. L. Gordon, A. C. Naveira Garabato, E. P. Abrahamsen, B. A. Huber, L. Jullion, and H. J. Venables (2011), Synchronous intensification and warming of Antarctic Bottom Water outflow from the Weddell Gyre, *Geophys. Res. Lett.*, *38*, L03603, doi:10.1029/2010GL046265.
Naveira Garabato, A. C., D. P. Stevens, and K. J. Heywood (2003), Water mass conversion, fluxes, and mixing in the Scotia Sea diagnosed by an inverse model, *J. Phys. Oceanogr.*, *33*(12), 2565–2587.
Naveira Garabato, A. C., L. Jullion, D. P. Stevens, K. J. Heywood, and B. A. King (2009), Variability of Subantarctic Mode Water and Antarctic Intermediate Water in the Drake Passage during the late-twentieth and early-twenty-first centuries, *J. Clim.*, *22*(13), 3661–3688.
Nowlin, W., and W. Zenk (1988), Westward bottom currents along the margin of the South Shetland Island Arc, *Deep Sea Res., Part A*, *35*(2), 269–301.
Palmer, M., D. Gomis, M. del Mar Flexas, G. Jordà, L. Jullion, T. Tsubouchi, and A. C. N. Garabato (2012), Water mass pathways and transports over the South Scotia Ridge west of 50°W, *Deep Sea Res., Part I*, *59*, 8–24.
Patterson, S. L., and H. A. Sievers (1980), The Weddell-Scotia confluence, *J. Phys. Oceanogr.*, *10*(10), 1584–1610.
Polzin, K. L., A. Garabato, E. P. Abrahamsen, L. Jullion, and M. P. Meredith (2014), Boundary mixing in Orkney Passage outflow, *J. Geophys. Res. Oceans*, *119*(12), 8627–8645.
Purkey, S. G., and G. C. Johnson (2013), Antarctic bottom water warming and freshening: Contributions to sea level rise, ocean freshwater budgets, and global heat gain, *J. Clim.*, *26*(16), 6105–6122.
Spencer, R., C. McGarry, A. Harrison, J. Vassie, T. Baker, M. Smithson, S. Haranzogo, and P. Woodworth (1993), The ACCLAIM programme in the South Atlantic and Southern oceans, *Int. Hydrogr. Rev.*, *70*, 7–21.
Su, Z., A. L. Stewart, and A. F. Thompson (2014), An idealized model of Weddell Gyre export variability, *J. Phys. Oceanogr.*, *44*(6), 1671–1688.
Su, Z., A. P. Ingersoll, A. L. Stewart, and A. F. Thompson (2016a), Ocean convective available potential energy. Part I: Concept and calculation, *J. Phys. Oceanogr.*, *46*(4), 1081–1096.
Su, Z., A. P. Ingersoll, A. L. Stewart, and A. F. Thompson (2016b), Ocean convective available potential energy. Part II: Energetics of thermobaric convection and thermobaric cabbeling, *J. Phys. Oceanogr.*, *46*(4), 1097–1115.
Thompson, A. F., K. J. Heywood, S. Schmidtko, and A. L. Stewart (2014), Eddy transport as a key component of the Antarctic overturning circulation, *Nat. Geosci.*, *7*(12), 879–884.
Visbeck, M. (2002), Deep velocity profiling using lowered acoustic Doppler current profilers: Bottom track and inverse solutions, *J. Atmos. Oceanic Technol.*, *19*(5), 794–807.
von Gyldenfeldt, A.-B., E. Fahrbach, M. A. Garcia, and M. Schröder (2002), Flow variability at the tip of the Antarctic Peninsula, *Deep Sea Res., Part II*, *49*(21), 4743–4766.
Wang, J., M. R. Mazloff, and S. T. Gille (2014), Pathways of the Agulhas waters poleward of 29°S, *J. Geophys. Res. Oceans*, *119*, 4234–4250, doi:10.1002/2014JC010049.
Watson, A. J., and A. C. Naveira Garabato (2006), The role of Southern Ocean mixing and upwelling in glacial-interglacial atmospheric CO_2 change, *Tellus, Ser. B*, *58*(1), 73–87.
Whitworth, T., W. Nowlin, A. Orsi, R. Locarnini, and S. Smith (1994), Weddell Sea shelf water in the Bransfield Strait and Weddell-Scotia confluence, *Deep Sea Res., Part I*, *41*(4), 629–641.
Williams, A., S. Bacon, and S. Cunningham (2006), Variability of the lower circumpolar deep water in Drake Passage 1926–2004, *Geophys. Res. Lett.*, *33*, L03603, doi:10.1029/2005GL024226.
Youngs, M. K., A. F. Thompson, M. M. Flexas, and K. J. Heywood (2015), Weddell Sea Export Pathways from Surface Drifters, *J. Phys. Oceanogr.*, *45*(4), 1068–1085.